

Large-Scale Monte Carlo Study of a Realistic Lattice Model for $\text{Ga}_{1-x}\text{Mn}_x\text{As}$.

Yucel Yildirim^{1,2}, Gonzalo Alvarez³, Adriana Moreo¹, and Elbio Dagotto¹

¹*Department of Physics and Astronomy, University of Tennessee, Knoxville, TN 37966-1200 and Oak Ridge National Laboratory, Oak Ridge, TN 37831-6032, USA,*

²*Department of Physics, Florida State University, Tallahassee, FL 32306, USA, and*

³*Computer Science and Mathematics Division, Oak Ridge National Laboratory, Oak Ridge, TN 37831-6032, USA.*

(Dated: August 15, 2018)

The properties of Mn-doped GaAs are studied at several doping levels and hole compensations, using a real-space Hamiltonian on an fcc lattice that reproduces the valence bands of undoped GaAs. Large-scale Monte Carlo (MC) simulations on a Cray XT3 supercomputer, using up to a thousand nodes, were needed to make this effort possible. Our analysis considers both the spin-orbit interaction and the random distribution of the Mn ions. The hopping amplitudes are functions of the GaAs Luttinger parameters. At the coupling $J \sim 1.2$ eV deduced from photoemission experiments, the MC Curie temperature and the shape of the magnetization curves are in agreement with experimental results for annealed samples. Although there are sizable differences with mean-field predictions, the system is found to be closer to a hole-fluid regime than to localized carriers.

PACS numbers: 75.50.Pp, 71.10.Fd, 72.25.Dc

Introduction. The study of diluted magnetic semiconductors (DMS) is a rapidly expanding area of research^{1,2,3,4,5} triggered by the discovery of high Curie temperatures (T_C) in some of these materials, and by their potential role in spintronics devices.⁶ Experimentally, much progress in the study of DMS was recently achieved after annealing techniques reduced the rates of compensation, allowing for higher T_C 's and for the intrinsic properties of DMS materials to be carefully investigated.⁷ Theoretical studies have focused on two idealized scenarios: (1) Impurity-Band (IB) models;⁸ and (2) Hole-Fluid (HF) models (based on mean-field approximations),^{2,9} which produce dramatic differences in most physical quantities.

These rather different views (1) and (2) of the same problem show that the use of unbiased computational techniques, such as lattice MC simulations, is crucial for progress in the modeling of DMS materials since it is unlikely that the coupling constants and densities locate the DMS systems exactly in one extreme or the other. Flexible methods that can interpolate between both limits within the same formalism are needed. However, while considerable progress has been achieved in numerical studies of simplified models¹⁰, the complexity of the real problem (involving several bands on an fcc lattice) has prevented its detailed analysis until now.

Here, we report a comprehensive numerical Monte Carlo study of a realistic lattice model for Mn-doped GaAs, including spin-orbit coupling, as well as the effects of random Mn doping. This large-scale computational effort was possible by using the Cray XT3 supercomputer operated by the National Center for Computational Sciences. Our simulations made use of up to 1,000 XT3 nodes. Parallelization was used in different ways: (i) to study different regions of parameter space (densities, couplings), and (ii) to average over different configurations of Mn locations. In all cases, the use of hundreds of processors in a single parallel run poses several techni-

cal challenges that are best handled by supercomputers with low latency and scalability, rather than by conventional clusters of PC's. In fact, this study would have taken several years without access to a supercomputer with thousands of processors, such as the Cray XT3.

The Model. We have constructed a real-space fcc-lattice Hamiltonian whose kinetic-energy term maps into the Luttinger-Kohn model,¹¹ when k -space Fourier transformed and at $k \rightarrow 0$. As a consequence, the hopping amplitudes are functions of (tabulated) Luttinger parameters, and thus they are precisely known.¹² To incorporate the spin-orbit (SO) interaction, we work in the $|j, m_j\rangle$ basis, where j can be $3/2$ or $1/2$ (since we consider the p orbitals, $l=1$, relevant at the Γ point of the GaAs valence band). Consequently, there are 6 possible values for m_j , indicating that this is a fully 6-orbital approach, arising from the 3 original p orbitals and the 2 hole spin projections. The Hamiltonian is formally given by

$$\begin{aligned} H = & \frac{1}{2} \sum_{\mathbf{i}, \mu, \nu, \alpha, \alpha', a, b} (t_{\alpha a, \alpha' b}^{\mu \nu} c_{\mathbf{i}, \alpha a}^\dagger c_{\mathbf{i}+\mu+\nu, \alpha' b} + \text{h.c.}) \\ & + \Delta_{SO} \sum_{\mathbf{i}, \alpha} c_{\mathbf{i}, \alpha \frac{1}{2}}^\dagger c_{\mathbf{i}, \alpha \frac{1}{2}} + J \sum_{\mathbf{I}} \mathbf{S}_{\mathbf{I}} \cdot \mathbf{S}_{\mathbf{I}}, \end{aligned} \quad (1)$$

where a, b take the values $\frac{1}{2}, \frac{3}{2}$ (for $j=3/2$), or $\frac{1}{2}$ (for $j=1/2$), and α and α' can be 1 or -1 . The Hund term describes the interaction between the hole spins $\mathbf{S}_{\mathbf{I}}$ (expressed in the $|j, m_j\rangle$ basis¹³) and the spin of the localized Mn ion $\mathbf{S}_{\mathbf{I}}$. The latter is considered classical ($|\mathbf{S}_{\mathbf{I}}|=1$),¹⁵ since it is large $S = 5/2$.¹⁶ $\mu + \nu$ are the 12 vectors indicating the 12 nearest-neighbor (NN) sites of each ion located at site \mathbf{i} , while \mathbf{I} are random sites in the fcc lattice. $\Delta_{SO}=0.341$ eV is the spin-orbit interaction strength¹⁷ in GaAs. The hopping parameters, $t_{\alpha a, \alpha' b}^{\mu \nu}$, are complex numbers, whose real and imaginary parts are functions of the Luttinger parameters.¹⁴

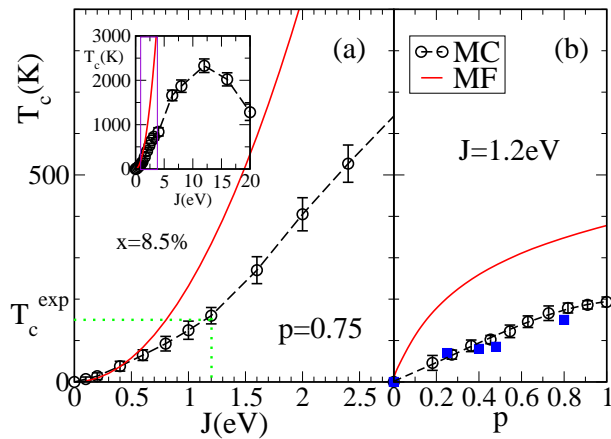


FIG. 1: (color online)(a) Curie temperature vs. J , for $x=8.5\%$ and $p\approx 0.75$. The MC results are indicated by circles, while the continuous line is the MF prediction.^{2,18} Inset: MC results for larger values of J to observe the crossover toward a localized picture. Vertical lines indicate the experimentally acceptable range of J . (b) MC calculated T_C vs. p , at $x=8.5\%$. The blue dots are experimental results,¹⁹ and the solid line the MF prediction.

Equation (1) can be studied with standard MC techniques for systems involving fermions and classical spins. These conceptually simple methods were already described in much detail in previous DMS investigations¹⁰ and also in manganese oxide studies, thus details will not be repeated here. Numerically, we analyze clusters that contain $N = N_x N_y N_z$ unit cells (N_i is the number of cells along the spatial direction i) of side a_0 ($a_0=5.64\text{\AA}$,¹⁷ is the *GaAs* cubic lattice parameter). Since in an fcc lattice there are 4 ions associated to each cell, the total number of *Ga* sites is $N_{Ga}=4N$. Since there are 6 single fermionic states per site, the diagonalization of a $6N_{Ga} \times 6N_{Ga}$ matrix is needed at each step of the MC simulation, which demands considerable computational resources for large enough clusters. The diagonalization can be performed exactly for values of N_{Ga} up to 500. We show below that lattices with $N_i = 4$ (256 sites) are large enough to study Mn dopings x and compensations p in the range of interest, with sufficient precision for our purposes. Nominally there should be one hole per Mn ion, but p can be smaller than 1 due to hole trapping defects, thus p and x are considered independent in this study.

Results. The highest T_C experimentally observed in bulk $\text{Ga}_{1-x}\text{Mn}_x\text{As}$ is $\sim 150\text{ K}$, at $x=8.5\%$ and $p\approx 0.7$.^{19,20} The system is metallic, and the magnetization vs. temperature displays mean-field behavior.¹⁹ In Fig. 1a, we present the (MC calculated) T_C as a function of the coupling J , at $x=8.5\%$ and $p\approx 0.75$. The results shown were obtained on lattices containing 256 (Ga,Mn) ions, and using an average over at least 5 different disorder configurations (only small differences were observed among the Mn configurations). Results for lattices with

up to 500 sites have also been calculated for some parameters (see below). At the realistic $J=1.2\text{ eV}$,²² Fig. 1a shows that the critical temperature is $T_C=155 \pm 20\text{ K}$. Since J is not accurately known, this excellent agreement with experiment¹⁹ could be partially fortuitous, but at least the results indicate that a reasonable quantitative estimation of the real T_C can be made via MC simulations of lattice models. The solid line in the figure corresponds to the MF results.^{2,18,23} The quantitative MF-MC agreement at small J provides a strong test of the reliability of the present MC approach. At $J=1.2\text{ eV}$, the MF T_C is $\sim 300\text{ K}$, showing that at these couplings and densities appreciable differences between MC and MF exist: the fluctuations considered in the MC approach cannot be neglected. The inset of Fig. 1 demonstrates that eventually for very large values of J the MF approximation breaks down, as expected. The MC simulations show that T_C reaches a maximum for $J \approx 12\text{ eV}$, of the order of the carriers bandwidth, and then it decreases due to the tendency of holes toward strong localization. This “up and down” behavior can only be obtained with lattice MC simulations valid at arbitrary values of J .¹⁰

At $J\sim 1.2\text{ eV}$ the system is closer to a hole-fluid than a localized regime as suggested by the magnetization vs. T curve, displayed in Fig. 2a. This curve has Curie-Weiss shape in qualitative agreement with both experimental results¹⁹ and previous MF calculations.^{9,18,23} This qualitatively correct shape of the magnetization curve was not obtained in previous lattice MC simulations.¹⁰ Size effects are mild as it can be seen in Fig. 3a where data for magnetization vs. T are presented for $x = 8.5\%$, $p \approx 0.75$, and $J = 1.2\text{ eV}$ in lattices with $(N_x, N_y, N_z) = (4, 3, 3)$, $(4, 4, 4)$, $(5, 4, 4)$, and $(6, 4, 4)$, i.e., with $N_{Ga}=144, 256, 320$, and 384 . Results for $N=500$ were obtained for lower doping (see Fig. 2b). Considering together the results for the different size clusters the estimated $T_C \approx 155 \pm 15\text{ K}$ is still in agreement with experiments (and also with the 256 sites results). Regarding the Curie-Weiss (CW) shape of the magnetization curve, we have phenomenologically observed that the finite spin-orbit coupling plays a crucial role in this respect. In Fig. 3b we show the magnetization vs. T for $x = 8.5\%$, $p = 0.75$, and $J = 1.2\text{ eV}$ for $\Delta_{SO} = 0.34\text{ eV}$ (squares) and $\Delta_{SO} = 0$ (circles): only the nonzero SO coupling produces CW behavior. In addition, we have noticed that the CW shape is also missing with the 4 orbital (with $j=3/2$) model that results in the limit $\Delta_{SO} \rightarrow \infty$.¹⁴ This indicates the important role that a realistic representation of the valence band plays in properly describing the thermodynamic observables.

The charge distribution in the cluster provides interesting information. In the HF scenario, the charge is assumed to be uniformly distributed while in the IB picture the charge is strongly localized. Fig. 3c indicates that in the realistic regime with $J = 1.2\text{ eV}$, $x = 8.5\%$, and $p \approx 0.75$ the charge is fairly uniformly distributed. The slightly darker points correspond to the sites where the Mn are located. They have charge of the order of

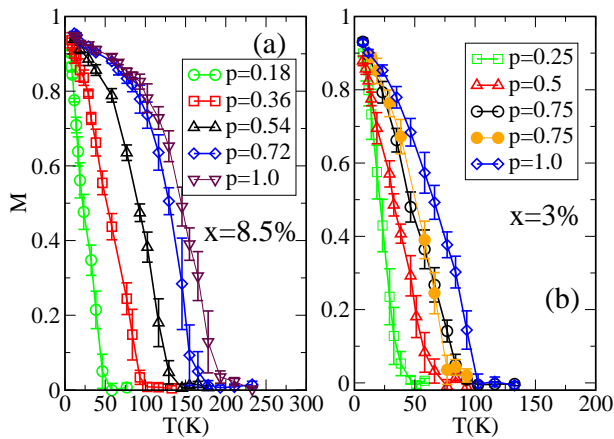


FIG. 2: (color online)(a) Magnetization M vs. T , for $x=8.5\%$ and several p 's (indicated, using a 256 sites lattice (open symbols)). Averages over 5 Mn-disorder configurations are shown. (b) Same as (a), but for $x=3\%$. Close circles are results for a 500 sites lattice. The magnetization is measured as $\mathcal{M} = \sqrt{\mathbf{M} \cdot \mathbf{M}}$, with \mathbf{M} the vectorial magnetization. As a consequence, for fully disordered spins, \mathcal{M} is still nonzero due to the $\mathbf{S}_i^2=1$ contributions, causing a finite value at large temperatures ($\mathcal{M}(T \rightarrow \infty) = 1/\sqrt{xN_{Ga}}$) unrelated to ferromagnetism. Thus, we plotted $M = (\mathcal{M} - \mathcal{M}(T \rightarrow \infty))/(1 - \mathcal{M}(T \rightarrow \infty))$, i.e. the background was subtracted.

20% above the MF value defined as $n_{MF} = n/N_{Ga}$ (with n the number of holes). As shown in Fig. 3d, charge localization occurs when J is increased to large values such as 12 eV. The dark circles at the Mn sites have charge intensities about 20 times the MF value, with very little charge found away from the impurities.

The lack of charge localization effects in the ordered state is concomitant with the absence of a notorious impurity band in the density-of-states (DOS) (Fig. 4a). Increasing J , an IB regime is eventually observed, given confidence that the study is truly unbiased. This occurs for $J \approx 4eV$ and beyond, with the IB becoming totally detached from the valence band at $J \approx 16eV$. Figures 3c, d and 4a show that the degree of spatial hole localization is correlated with the development of the IB. In addition, when the holes are localized, the M vs. T curves present substantial deviations from MF behavior (not shown), with a different concavity as that of Fig. 2a.¹⁰

It is well known that the carrier density in DMS is strongly dependent on sample preparation. Due to defects, p is much smaller than 1 in most samples. In Fig. 1b, the MC calculated T_C vs p for $x=8.5\%$ and $J=1.2eV$ is shown. T_C increases with p , and it reaches a maximum at $p \sim 1$ as in previous theoretical,^{2,10} and experimental results^{7,19,25,27} also shown in the figure. The agreement between MC results and experiments is once again quite satisfactory. The figure suggests that if $p=1$ were reachable experimentally, then T_C could be as high as ~ 200 K. We also observed qualitative changes in the

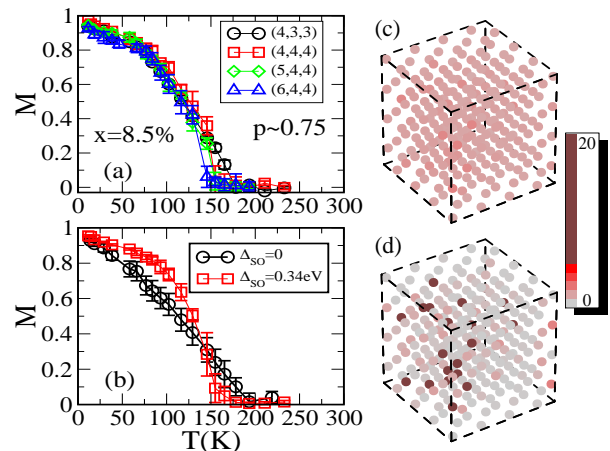


FIG. 3: (color online)(a) M (defined as in Fig. 2) vs T for different lattice sizes for $x = 8.5\%$, $p \approx 0.75$, and $J = 1.2eV$; (b) M vs. T for the same parameters as in (a) on a 256 sites lattice with (without) spin-orbit interaction indicated by the squares (circles); (c) Charge density normalized to the MF value (see text), for $x = 8.5\%$, $p \approx 0.75$, $T=10K$, on a 256-sites cluster for $J=1.2eV$. The color intensity is proportional to the charge density (see scale). (d) Same as (c), but for $J=12eV$.

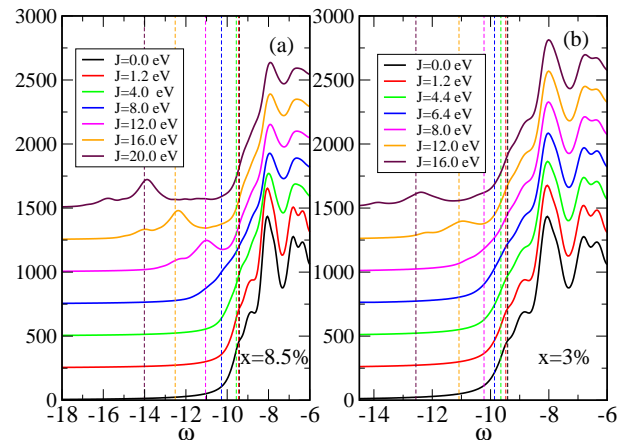


FIG. 4: (color online)(a) Density-of-states, for $x=8.5\%$, $p \approx 0.75$, and several J 's. The dashed vertical lines indicate the position of the chemical potentials. (b) Same as (a) but for $x = 3\%$.

magnetization curve varying p (Fig. 2a): as p is reduced, the magnetization changes from a Brillouin form to an approximately linear shape with T . In fact, the observed p dependence is once again similar as found experimentally, with p modified by annealing;¹⁹ the Mn disorder plays a more dominant role when the number of holes is reduced. In spite of the deviations from MF behavior at small p , we could not observe a clear IB as p was reduced, for the coupling J used in our analysis.

Consider now the low Mn-doping regime. The latest experimental results suggest that (Mn,Ga)As should still be metallic at $x=3\%$.²⁵ A metal-insulator transition is expected at $x \leq 1\%$,²⁶ but MC studies for such very small dopings need much larger clusters than currently possible. Our MC simulations indicate that at low Mn-doping, the dependence of T_C with J is similar as in the higher doping case.

No clearly formed IB is observed in the $x=3\%$ DOS displayed in Fig. 4b: the IB's are formed for similar values of J with increasing J , at both $x=3\%$ and 8.5% , as deduced from an analysis of fermionic eigenvalues for spin-ordered configurations.^{14,29}

Summary. Here, a MC study of an fcc lattice model for DMS compounds, including the realistic valence bands of GaAs, the spin-orbit interaction, and the random distribution of Mn dopants has been presented. The use of the Cray XT3 at ORNL made this effort possible. The results show magnetizations and T_C 's in reasonable agreement with experiments. The simulations show that the carri-

ers tend to spread over the entire lattice, and they reside in the valence band at realistic couplings, qualitatively in agreement with MF^{2,9} and first principles⁵ calculations in the same parameter regime, as well as with experimental data on annealed samples.^{7,25} However, an IB band populated by a fraction $1-p$ of trapped holes that do not participate in the transport properties is not ruled out by our results. The MC method described here opens a new semi-quantitative window for theoretical research on the properties of DMS materials.

Acknowledgments. We acknowledge discussions with T. Dietl, A. MacDonald, J. Sinova, T. Schulthess, F. Popescu and J. Moreno. Y.Y., A.M., and E.D. are supported by NSF under grants DMR-0443144 and DMR-0454504. G.A. is sponsored by the Division of Materials Sciences and Engineering, Office of Basic Energy Sciences, U.S. Department of Energy, under Engineering, Office of Basic Energy Sciences, DOE, under contract DE-AC05-00OR22725 with ORNL, managed and operated by UT-Battelle, LLC.

-
- ¹ H. Ohno, *Science* **281**, 951 (1998).
² T. Dietl, *et al.*, *Science*, **287**, 1019 (2000).
³ T. Jungwirth *et al.*, *Rev. Mod. Phys.* **78**, 809 (2006).
⁴ A. MacDonald *et al.*, *Nature Materials* **4**, 195 (2005).
⁵ T. Schulthess *et al.*, *Nature Materials* **4**, 838 (2005).
⁶ I. Zutic *et al.*, *Rev. Mod. Phys.* **76**, 323 (2004).
⁷ S. J. Potashnik *et al.*, *Appl. Phys. Lett.* **79**, 1495 (2001).
⁸ M. Berciu and R. Bhatt, *Phys. Rev. Lett.* **87**, 107203 (2001).
⁹ M. Abolfath, T. Jungwirth, J. Brum and A. MacDonald, *Phys. Rev.* **B63** 054418 (2001).
¹⁰ One-band models were studied in G. Alvarez *et al.*, *Phys. Rev. Lett.* **89**, 277202 (2002) and M. Mayr *et al.*, *Phys. Rev.* **B65**, 241202(R) (2002); two-band models in F. Popescu *et al.*, *Phys.Rev.* **B73**, 075206 (2006); MC results for the kinetic-exchange model are in J. Schliemann *et al.*, *Phys. Rev.* **B64**, 165201 (2001); and LSDA-based estimations of T_C are in J. Xu *et al.*, *Phys. Rev. Lett.* **84**, 097201 (2005).
¹¹ J.M. Luttinger and W. Kohn, *Phys. Rev.* **97**, 869 (1955).
¹² J.M. Luttinger, *Phys. Rev.* **102**, 1030 (1956). The hoppings used in our study are all of order 1 eV.
¹³ These are 6×6 matrices; see Eq.(A.10) (in Ref.9) and 14.
¹⁴ Details will be published elsewhere (in preparation).
¹⁵ The classical limit corresponds to $\lim_{\hbar \rightarrow 0, S \rightarrow \infty} \hbar S = \hbar_0 = 6.58 \times 10^{-16}$ eV s. Since the parameter J , experimentally measured, is proportional to \hbar via the Bohr magneton, it results that $J = K\hbar$ where K is a constant. Thus, $\lim_{\hbar \rightarrow 0, S \rightarrow \infty} JS = \lim_{\hbar \rightarrow 0, S \rightarrow \infty} K\hbar S = K\hbar_0 = J$. See G. Q. Pellegrino, K. Furuya, and M.C. Nemes, *Chaos* **5** 463 (1995); G.Q. Pellegrino, K. Furuya, and M.C. Nemes, *Revista Brasileira de Ensino de Fisica* **20**, 321 (1998); L.G. Yaffe, *Rev. Mod. Phys.* **54**, 407 (1982). This approach is also supported by comparisons of our numerical data with MF calculations for the quantum case.
¹⁶ J. Szczytko *et al.*, *Phys. Rev.* **B60**, 8304 (1999); M. Linarsson *et al.*, *Phys. Rev.* **B55**, 6938 (1997); O.M. Fedorych *et al.*, *Phys. Rev.* **B66**, 045201 (2002).
¹⁷ Peter Yu and Manuel Cardona, *Fundamentals of Semiconductors*, Third Edition, Springer-Verlag.
¹⁸ T. Dietl, private communication.
¹⁹ K.C. Ku *et al.*, *Appl. Phys. Lett.* **82**, 2302 (2003).
²⁰ T. Jungwirth *et al.*, *Phys.Rev.* **B72**, 165204 (2005); K.Y. Wang *et al.*, *AIP Conf. Proc.* **772**, 333 (2005).
²¹ N=500 results were obtained for lower doping (Fig. 2b).
²² J. Okabayashi *et al.*, *Phys. Rev.* **B58**, R4211 (1998).
²³ T. Dietl *et al.*, *Phys.Rev.* **B63**, 195205 (2001).
²⁴ John Schliemann *et al.*, *Appl. Phys. Lett.* **78**, 1550 (2001).
²⁵ K.W. Edmonds *et al.*, *Appl. Phys. Lett.* **81**, 3010 (2002).
²⁶ S.-R. Yang and A.H. MacDonald, *Phys. Rev.* **B67**, 155202 (2003).
²⁷ S.J. Potashnik *et al.*, *Phys. Rev.* **B66**, 012408 (2002).
²⁸ J. Okabayashi *et al.*, *Phys. Rev.* **B64**, 125304 (2001); J. Okabayashi *et al.*, *Physica* **E10**, 192 (2001).
²⁹ *Coulomb interaction.* While the J term in Eq.(1) is crucial for ferromagnetism, it is expected that most of the carrier binding energy, at least at very low doping, originates from the attraction between the Mn ions and the hole carriers. To mimic this attractive Coulomb interaction, we added to Eq.(1) a term of the form $H_{Coul} = V \sum_{\mathbf{I}} n_{\mathbf{I}}$, using values of V up to 2 eV, which is needed to generate the ~ 0.1 eV binding energy of (Mn,Ga)As. At small J , V tends to effectively *increase* J , since it increases the chances for the carriers to interact locally with the Mn spins. As a consequence, adding a Coulomb attraction as described above, does not generate a case at $x=8.5\%$ or 3% , presenting both an IB and a T_C close to the experimental range. It is possible though that the Coulomb attraction develops an IB for smaller values of x (in the insulating regime¹⁷) that cannot be studied with our finite clusters. Details will be presented elsewhere.³⁰
³⁰ F. Popescu *et al.*, in preparation.